Current Opinion in Solid State and Materials Science 25 (2021) 100936

Contents lists available at ScienceDirect

Current Opinion in Solid State & Materials Science

journal homepage: www.elsevier.com/locate/cossms

# Polymer derived ceramic aerogels

Cekdar Vakifahmetoglu [a,*], Tugce Semerci [a], Aleksander Gurlo [b], Gian Domenico Soraru [c]

[a] Department of Materials Science and Engineering, Izmir Institute of Technology, 35430 Urla, Izmir, Turkey
[b] Fachgebiet Keramische Werkstoffe/Chair of Advanced Ceramic Materials, Institut für Werkstoffwissenschaften und technologien, Technische Universitaet Berlin, 10623, Germany
[c] Department of Industrial Engineering, University of Trento, Via Sommarive 9, 38123 Trento, Italy

ARTICLE INFO

*Keywords:*
Aerogel
Drying
Polymer derived ceramics
Porous materials

ABSTRACT

Aerogels are unique porous solids having exceptional low relative density together with high specific surface area, making them very attractive materials for scientific research and industrial applications. Polymer derived ceramic aerogels are a new class of materials obtained through the pyrolysis of sol-gel/preceramic polymers. Herein this review, some of the representative formation methods and applications of polymer derived ceramic aerogels are highlighted with a specific focus on the thermal, electrical, and adsorbent related properties.

## 1. Introduction & brief definitions

Aerogels are highly porous and thus extremely light components consisting of mostly air in their 3D solid networks; an ultra-low density, 0.00016 g/cm$^3$, carbon aerogel example standing on *Setaria viridis* is shown in Fig. 1(a). Since their introduction to the scientific community in the 1930s [1], a considerable research effort has been devoted to explore novel compositions because of their unique properties, especially very low density (<0.5 g/cm$^3$), high porosity (usually > 90%), high surface area (usually ~100–1000 m$^2$/g) and low thermal conductivity (<0.05 W m$^{-1}$ K$^{-1}$ at room temperature (RT)), making them an excellent choice for energy storage [2], thermal insulation [3,4], sensor [5–8] and wastewater treatment [9,10] applications.

### 1.1. Aerogel processing

Virtually all aerogels are produced by sol-gel technique following four important stages: sol and gel preparation, aging, and drying. Gel formation starts, first, with the hydrolysis of the precursor and then its condensation leads to the formation of a sol, i.e., to the dispersion of colloidal particles in the solution. After that, condensation reactions proceed, and a network of colloidal particles becomes a *gel*. After that, in the aging stage, the solid network is reinforced as the reaction progresses to completion. While the main aim of the drying process is to remove the solvent from the gel, depending on the selected drying path xerogels/ambigels, cryogels and aerogels can be formed by ambient pressure, freeze, and supercritical drying. It is important to emphasize that the terminology describing what is an aerogel is not yet standardized and can be confusing. Starting from a gel that is not significantly affected by the drying process, one could obtain materials having basically the same microstructures by following different drying processes. Therefore, here in this review, aerogels are defined in a broad perspective as *highly porous solids dried from gels without a collapse or significant destruction of the pore structure.*

The simplest drying route is the solvent removal by evaporation under ambient conditions, resulting in the formation of xerogel. Under atmospheric pressure and at low temperatures (generally below 100 °C), the structure is exposed to unconstrained shrinkage because of the high surface tension of the solvent, i.e., capillary forces occurring during drying, and thus processing speed/conditions should be carefully controlled to minimize the flaws. It is important to note that aerogel-like materials (meaning that properties are more like aerogels than those of xerogels) are also produced by ambient pressure drying instead of supercritical drying route [11–13]. For this purpose, to decrease the liquid/vapor interfacial energy, the liquid can be exchanged with a solvent having low surface tension. Besides, one can consider applying additional treatments (e.g., utilization of *drying control chemical additives* (DCCA) [14]), to reduce the stresses created by these drying conditions, and under such settings the formed material is called *ambigel* [15].

In freeze-drying, the solvent is first frozen and then it is removed by sublimation to obtain cryogel. Finally, in the most commonly applied supercritical drying, the solvent is removed under supercritical conditions, higher than the critical temperature and pressure of the used solvent, to produce aerogel without the collapse of the matrix. This stage

* Corresponding author.
*E-mail addresses:* cekdarvakifahmetoglu@iyte.edu.tr, cvahmetoglu@gmail.com (C. Vakifahmetoglu).

https://doi.org/10.1016/j.cossms.2021.100936
Received 5 January 2021; Received in revised form 5 May 2021; Accepted 6 May 2021
Available online 19 May 2021

is based on minimizing the pore shrinkage caused by the capillary forces.

Among the available solvents, carbon dioxide ($CO_2$) is the most widely used for supercritical drying because it is not only cost-effective, non-toxic, and non-explosive but also the requirements to bring it to supercritical conditions are relatively simple [16]. Besides, at the temperatures of use, it is actually inert contrary to some others for which super-critical conditions may also impose reactions that can be advantageous or disadvantageous but certainly affect the final product. In the $CO_2$ supercritical drying route, the gel is placed in a pressure vessel, filled with liquid $CO_2$, and solvent in the gel is periodically replaced with the liquid $CO_2$. Subsequently, the vessel is brought to a supercritical region with critical temperature (31 °C) and pressure (7.37 MPa) of $CO_2$. Then applied pressure and temperature are decreased to remove the available $CO_2$, see the liquid-gas transition path shown in Fig. 1(b). In the supercritical region, there is no discrimination in liquid/vapor phase since the surface tension becomes negligible, i.e., the pore network is not exposed to shrinkage and a probable collapse.

There are also other drying techniques such as subcritical drying at which the liquid surface tension is low or drying by microwave heating in which the inward travelling energy interacts with molecules and vaporizes the confined liquid before leaving. The latter system results in faster drying than that of the classical drying via evaporation in which initially the surface solvent layer is removed and the remaining liquid diffuses to the surface (generally long drying time for completion) [17,18]. Further details on the formation of the broadly called aerogel systems can be followed from recent books [19,20] and comprehensive reviews [21–26].

### 1.2. Common aerogel types

Silica and carbon are by far the most investigated aerogel types, but there are many others including polymeric ones such as polyvinylchloride [29], polyimide [30–32], polyvinylidene-fluoride [33]. Composites, for example, polyvinylidene-fluoride/silica [34], polymethylmethacrylate/silica [35], and ceramics like $Si_3N_4$ [36,37], SiC [38], YSZ [39], etc. However, due to inherent difficulty to process ceramics as aerogels by conventional ceramic formation techniques (limited crosslinking between ceramic building blocks), only a limited number of chemical compounds were able to be produced at present [40].

## 2. Precursor derived ceramic aerogels

It is possible to produce a variety of aerogels, belonging to the general Si-O-C-N-B system following the well-established precursor or polymer derived ceramic (PDC) route. PDC aerogels are a new class of materials obtained through preceramic polymer pyrolysis. This processing approach has distinct advantages, the most important of which is the low processing temperatures, i.e., they can be formed very easily by cost effective techniques (compression/injection molding, spinning, extrusion, etc.). Besides, they do not need sintering additives, and the obtained materials show enhanced creep resistance and thermal stability up to at least 1200 °C when compared with that of the similar compositions formed by following conventional methods [41–43]. In the PDC aerogel production process, some differences may exist, such details can be followed from a comprehensive chapter which was specifically focused on the synthesis [44], here in addition to the properties collected from the published works, only brief information for the synthesis of few compositions will be indicated.

One of the first publications in this regard was done by Aravind and Soraru [45] about sol-gel derived and ambient pressure dried aerogel-like structures (ambigels) which were pyrolyzed to form highly porous SiOC parts in 2010. A wide variety of decade-long works demonstrated the fruitfulness of the route and the formation of several other ceramic aerogel types in the PDC family (SiOC, SiC, SiC/C, SiCN, etc.), as detailed in Tables 1–3. It is presumed that PDC aerogel formation is akin to the precipitation polymerization of polymeric monodisperse particles [46], nevertheless, there is no conclusive research on the exact formation mechanism. Accordingly, the papers in which the authors claimed to form aerogels by using preformed 1D nanostructure (e.g., SiC nanofibers) as building blocks instead of dispersed particles or gels, are separately placed at the bottom of the tabulated data. This is because, in these works, components analogous to aerogels and having attractive properties, for instance, very low bulk density ~0.04 g/cm$^3$ and a distinctive recoverable strain reaching ~40% [47] were demonstrated.

### 2.1. Sol-gel and polymer processing of aerogels

To the best of our knowledge, all PDC aerogels were produced either by (i) sol-gel chemistry or (ii) preceramic polymer processing. Sol-gel route involves the primary synthesis step for the required preceramic polymer by using hybrid silicon alkoxides including tetraethylorthosilicate [48–50], methyldimethoxysilane [49], methyl-, ethyl-, propyl- and phenyl-trimethoxysilane [48,49,51]. These alkoxides are typically dissolved in ethanol and hydrolyzed with water to promote hydrolysis/condensation reactions. One of the main advantages of this route is the possibility to blend different alkoxides to fine tune the composition of the resulting preceramic network in terms of Si/C/O atomic ratio. Controlling the composition of the precursor allows achieving, after pyrolysis, silicon oxycarbide ceramics with defined amounts of Si-C, Si-O bonds, and free carbon [52–54]. Moreover, further elements (B, Ti, Al, Zr, etc.) can be homogeneously introduced in the siloxane network in the sol-gel process using the corresponding alkoxides to obtain multicomponent silicon oxycarbide glasses; Si-Metal-O-C [55,56]. Instead, when commercial preceramic polymers were used, aerogel processing is simpler since there is no need to synthesize the starting precursor. There are readily available, commercial preceramic polymers, and among them, polysiloxanes, polysilazanes, and polycarbosilanes are the most employed ones.

Apart from the differences in the initial synthesis procedure, the rest of the processing follows the common steps. The crosslinking of the

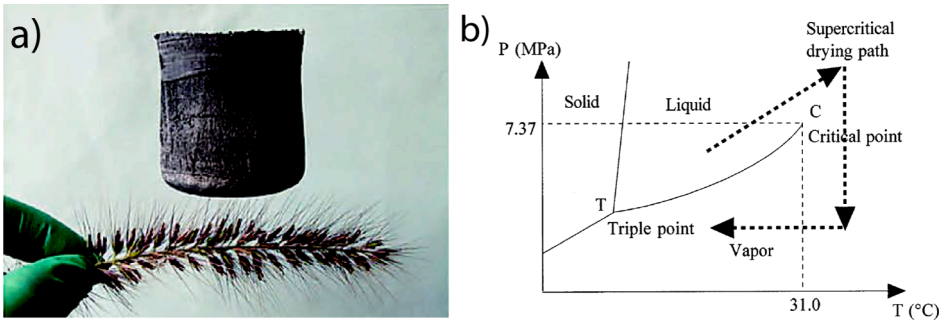


**Fig. 1.** (a) Ultra-low density (0.00016 g/cm$^3$) carbon aerogel on Setaria viridis plant (Reproduced from [27] with permission John Wiley and Sons, Copyright 2013), and (b) $CO_2$ unary phase diagram (Reproduced from [28] with permission American Chemical Society, Copyright 2002).

**Table 1**
Precursor type (sol-gel and commercial preceramic polymer), processing parameters, and observed properties of SiOC-based aerogels. Apart from porosity related properties such as pore volume and diameter, surface area, additional features are collectively given under *other properties* column (valid for other tables as well).

| PDC aerogel | Processing parameters | | | Pore properties | Other properties | Possible applications | Ref. |
|---|---|---|---|---|---|---|---|
| | Solvent | Drying method | Pyrolysis | | | | |
| **Commercial preceramic polymer** | | | | | | | |
| SiOC | ACE | Supercritical drying [$CO_2$] | 1000 °C<br>1 h<br>Ar | Ø = 24 nm<br>SSA = 180 $m^2/g$<br>$V_{pore}$ = 1.09 $cm^3/g$ | $Q_{insertion}$ = 1280 $mAhg^{-1}$<br>$Q_{extraction}$ = 600 $mAhg^{-1}$<br>$Q_{irreversible}$ = 680 $mAhg^{-1}$<br>(@C(360$mAg^{-1}$)<br>η = 47–99% | Anode for Li-ion batteries | [72] |
| SiOC | ACE | Supercritical drying [$CO_2$]<br>(8 days/<br>41 °C/<br>95 bar) | 1200–1300 °C<br>5 h<br>Ar | Ø < 10 nm & 10–50 nm<br>SSA = 33–530 $m^2/g$<br>$V_{pore}$ = 0.14–0.65 $cm^3/g$ | N.A. | N.A. | [63] |
| SiOC | ACE & Cy | Supercritical drying [$CO_2$]<br>(4 days/<br>45 °C) | 900 °C<br>1–7 h<br>Ar & $H_2$/Ar | Ø < 10 nm & 20–30 nm<br>SSA = 87–215 $m^2/g$<br>$V_{pore}$ = 0.15–0.87 $cm^3/g$<br>$\rho_b$ ~ 0.65–0.98 $g/cm^3$ | $Q_{reversible}$ ~ 900 $mAhg^{-1}$ (@C(360$mAg^{-1}$))<br>η = 35–52% | Anode for Li-ion batteries | [60] |
| SiOC | ACE | Supercritical drying (N.A.) | 800 - 1600 °C<br>2 h<br>$N_2$ | SSA = 48–227 $m^2/g$<br>$V_{pore}$ = 0.18–0.29 $cm^3/g$<br>$\rho_b$ ~ 0.51–1.14 $g/cm^3$ | N.A. | N.A. | [73] |
| SiOC & SiC | ACE & Cy | Supercritical drying [$CO_2$] | 900 °C<br>1 h<br>Ar | $\phi_T$ = 72–86%<br>Ø = 10–90 nm<br>SSA = 102–163 $m^2/g$<br>$V_{pore}$ = 0.39–0.72 $cm^3/g$ | $R_{ads}$ = 100% @$C_o$ = 1 mg/L (SiOC & SiC)<br>$q_m$ = 44.2 mg/g (SiOC) | Water purification | [74] |
| SiOC & SiCN | ACE & Cy | Supercritical drying [$CO_2$]<br>(5 days/<br>45 °C/<br>100 bar)<br>&<br>Ambient pressure<br>(3 days) | 900–1300 °C<br>$N_2$<br>$CO_2$<br>$NH_3$ | Ø = 5–200 nm<br>SSA = 30–388 $m^2/g$<br>$V_{pore}$ = 0.21–0.84 $cm^3/g$<br>$\rho_b$ ~ 0.45–0.70 $g/cm^3$ | $q_m$ ~ 10 mg/g (Cr(III))<br>$q_m$ ~ 20–30 mg/g (Cr(VI)) | Water purification | [64] |
| **Sol-gel synthesized materials** | | | | | | | |
| SiOC | IPA | Ambient pressure<br>(21 days/<br>50 °C) | 1000 °C<br>3 h<br>Ar | Ø ~ 3–24 nm<br>SSA = 132–452 $m^2/g$<br>$V_{pore}$ = 0.33–0.89 $cm^3/g$ | N.A. | N.A. | [45] |
| SiOC | IPA | Ambient pressure<br>(21 days/<br>50 °C) | 1400 °C<br>3 h<br>Ar | Ø = 2–20 nm<br>SSA = 150 $m^2/g$<br>$V_{pore}$ = 0.19 $cm^3/g$ | $\tau_{resp}$ = 4 min (@5ppm $NO_2$)<br>5 min. (@5000 ppm $H_2$)<br>$\tau_{rec}$ = 2 min. (@5ppm $NO_2$)<br>1 min. (@5000 ppm $H_2$) | Gas sensor<br>(for $NO_2$, $H_2$, detection) | [67] |
| SiOC | IPA | Ambient pressure<br>(21 days/<br>50 °C) | 800 - 1100 °C<br>1 h<br>$H_2$ | Ø ~ 2–6 nm<br>SSA = 171–615 $m^2/g$<br>$V_{pore}$ = 0.18–0.58 $cm^3/g$<br>$\rho_b$ ~ 0.90–1.30 $g/cm^3$ | R = 55–78% (@ > 600 nm)<br>R = 20–67% (@ 400 nm) | Optical sensor | [68] |
| SiOC | IPA | Ambient pressure<br>(2 days/<br>60 °C) | 1000 °C<br>1 h<br>Ar | Ø = 2 nm & 95–350 nm<br>SSA = 354–488 $m^2/g$<br>$\rho_b$ = 0.27–0.34 $g/cm^3$ | $\sigma_c$ = 1.45–3.17 MPa | N.A. | [69] |
| SiOC | EtOH | Supercritical drying [$CO_2$]<br>(4 h/<br>35 °C/<br>80 bar) | 1000 - 1600 °C<br>1 h<br>Ar | Ø = 10–1000 nm<br>SSA = 10–247 $m^2/g$ | N.A. | N.A. | [75] |
| SiOC | | | | | | N.A. | [76] |

(*continued on next page*)

**Table 1** (*continued*)

| PDC aerogel | Processing parameters | | | Pore properties | Other properties | Possible applications | Ref. |
|---|---|---|---|---|---|---|---|
| | Solvent | Drying method | Pyrolysis | | | | |
| | EtOH & HCl acid | Supercritical drying [$CO_2$] | 1000 °C 2 h Ar | Ø ~ 9 nm SSA = 531 $m^2/g$ $V_{pore}$ = 0.97 $cm^3/g$ $\rho_b$ = 0.4 $g/cm^3$ | E = 1.42 GPa G = 0.54 GPa | | |
| SiOC | IPA | Supercritical drying [EtOH] | 1200 °C 1 h Ar | Ø = 56 nm SSA = 198 $m^2/g$ $V_{pore}$ = 0.65 $cm^3/g$ $\rho_b$ = 0.3 $g/cm^3$ | $\lambda$ = 0.027 W $m^{-1}$ $K^{-1}$ @RT | Thermal insulation | [77] |
| SiOC/BN | NHEX | Ambient pressure (3 days/ 60 °C) | 900–1300 °C 2 h $N_2$ | Ø = 10–20 nm & < 69 nm SSA = 27–566 $m^2/g$ $V_{pore}$ = 0.26–1.12 $cm^3/g$ $\rho_b$ = 0.36–0.89 $g/cm^3$ | $\lambda$ ~ 0.040–0.200 W $m^{-1}$ $K^{-1}$ @RT $\lambda$ ~ 0.150–0.750 W $m^{-1}$ $K^{-1}$ @1300 °C $\sigma_c$ = 2.2–20.3 MPa | Thermal insulation | [70] |
| SiBOC | EtOH | Supercritical drying (N.A.) | 1200 °C | Ø = 10–150 nm SSA = 293 $m^2/g$ | $\lambda$ = 0.138 W $m^{-1}$ $K^{-1}$ (in vacuum @1500 °C) $\sigma_c$ ~ 1.849 MPa, $\varepsilon$ ~ 20% | Thermal insulation | [78] |
| SiOCN | EtOH | Freeze drying & Vacuum drying (80 °C) | 450 - 900 °C 2 h $N_2$ | Ø ~ 3–12 nm SSA ~ 25–827 $m^2/g$ | $\eta$ = -8–75.9% | Volatile carbonyl compound adsorbent & cigarette smoke filter | [79] |

N.A. = Not available, Ø = pore diameter, $\phi_T$ = total porosity, SSA = specific surface area, $V_{pore}$ = Pore volume, $\rho_b$ = bulk/apparent density, $\sigma_c$ = compressive strength, $\varepsilon$ = strain, $\lambda$ = thermal conductivity, E = Young's modulus, G = shear modulus, Q = specific capacity, $\eta$ = efficiency, $\tau_{resp}$ = response time, $\tau_{rec}$ = recovery time, R = reflectance, $R_{ads}$ = % adsorbent, $C_o$ = initial concentration, $q_m$ = max. adsorption capacity, ACE = acetone, Cy = cyclohexane, EtOH = ethanol, HCl acid = hydrochloric acid, IPA = isopropanol, NHEX = n-hexane.

precursors forming a gel is done in an autoclave or a closed system to prevent the evaporation of the solvent (as known the used solvents have low boiling points). In the next stage, the obtained wet gel is periodically washed to remove the residuals (precursor, catalyst, etc.), followed by pivotal drying step including supercritical, freeze, and ambient pressure drying. Unconventional drying methods such as microwave or subcritical drying have not been applied via the PDC route yet. Finally, the obtained dry polymeric aerogel is pyrolyzed yielding a PDC aerogel.

It was shown that the microstructure of the PDC aerogels can be altered by controlling the dilution level and the type of solvent. Briefly, increasing the dilution causes an increase both in pore and particle size. The reason behind such an issue might be a decrease in the polymerization rate, i.e., the nucleation rate of the particles [44]. Accordingly, enhanced total porosity and pore size of SiOCN aerogel was obtained when the higher volume of cyclohexane solvent was used [57]. Increasing the solvent solubility causes a larger pore size as well [44], although the exact reason for this measure is still unclear. In this regard, the effect of different solvents on the microstructural evolution of poly (methylhydrosiloxane)/divinylbenzene (PMHS/DVB) aerogels was studied. It was postulated that both swelling and solubility of the crosslinked preceramic polymer in various solvents were important to govern the final porosity characteristics. The reported SSA and average pore size of the aerogels obtained by using acetone were 392 $m^2/g$ and 18.8 nm, respectively, which was higher than that of cyclohexane used ones (120 $m^2/g$ and 14.7 nm) [58]. Furthermore, the effect of supercritical drying temperature (40–50 °C for $CO_2$) was also examined but the results did not give a clear trend [59].

While dilution level and the solvent type are important, unless it is a reactive atmosphere (such as $H_2$, $NH_3$, or $CO_2$) [60,61], there was no clear effect on the microstructural evolution when the "inert" pyrolysis atmosphere was altered. It should be noted here that due to the high permeability and high specific surface area of the polymeric aerogels, the preceramic network is highly prone to react with the $O_2$/$H_2O$ during pyrolysis. Accordingly, initially long inert gas purging time should be employed to remove moisture/oxygen in the tube, and a special specific care should be given throughout the manufacturing when oxygen is considered as an impurity [44].

The plot given in Fig. 2 (right) displays the drying time/pore size data extracted from published studies (see Tables 1–3 as well). While freeze drying is the fastest drying method, it may take as long as 21 days via ambient pressure. Besides, generally speaking for the PDC route, aerogels with average pore sizes below 200 nm have been produced. It is worth to underline that most of the presented data was collected only by using $N_2$ sorption analysis, and the accurately measurable pore size limit of the technique is already around the given upper boundary [62].

### 2.2. SiOC-based aerogels

Among all, Silicon Oxycarbide (SiOC) is the most widely studied polymer derived ceramic composition because its precursors are the most economical ones, they are readily available, and can be handled and processed in an ambient atmosphere. As can be seen from Table 1, for SiOC aerogels, pore sizes in the range from 2 to few hundred nanometers, specific surface area (SSA) reaching around 600 $m^2/g$, and total porosity up to 96 vol% have been documented. Apparently, sol-gel chemistry is the most applied technique to synthesize SiOC aerogels.

In a particularly intriguing study demonstrated the formation of transparent and colorless SiOC aerogels. The authors used bis(triethoxysilyl)methane (BTEM) and bis(triethoxysilyl)ethane (BTEE) as precursors for acid/base sol-gel formation, followed by the pyrolysis at 800 °C under pure hydrogen ($H_2$) atmosphere. Fig. 3(a)–(f) show the photographical images of the samples obtained in the study under different pyrolysis temperatures [68]. It was shown that $H_2$ reacts with the organic side groups of polymers reducing in this way the amount of carbon in the formed PDC component [45,71]. Considering the observed variety of properties in Table 1, it is possible to state that SiOC aerogels can be considered for several applications, including as anodes for lithium-ion batteries, gas and optical sensors, and adsorbents for water purification.

### 2.3. SiCN-based aerogels

Although the final material yield was probably very low, an appealing N-doped carbide derived carbon (N-doped CDC) aerogel was obtained by using polysilazane derived SiCN aerogel as a substrate to be etched by halogen gas (chlorine). The produced aerogel with a high

**Table 2**
Processing parameters and observed characteristics for preceramic polymer derived SiCN-based aerogels.

| PDC aerogel | Processing parameters | | | Pore properties | Other properties | Possible applications | Ref. |
|---|---|---|---|---|---|---|---|
| | Solvent | Drying method | Pyrolysis | | | | |
| **Commercial preceramic polymer** | | | | | | | |
| SiCN | Cy | Supercritical drying [$CO_2$] (4 days/ 50 °C/ 100 bar) | 1000–1500 °C 1 h $N_2$ | $\phi_T$ = 95–96% Ø ~ 30–40 nm SSA ~ 153–165 $m^2/g$ $V_{pore}$ = 0.56–0.58 $cm^3/g$ | N.A. | N.A. | [82] |
| SiCN | Cy | Supercritical drying [$CO_2$] (5 days/ 45 °C/ 100 bar) | 450 - 1000 °C 1 h Ar | Ø = 3–100 nm SSA = 75–725 $m^2/g$ $V_{pore}$ = 0.24–0.83 $cm^3/g$ | N.A. | N.A. | [65] |
| SiCN | Cy | Freeze drying (-78 °C/24 h) | 1000–1400 °C 2 h $N_2$ | Ø ~ 18–22 nm SSA ~ 106–235 $m^2/g$ $V_{pore}$ = 0.49–0.56 $cm^3/g$ $\rho_b$ ~ 0.19 $g/cm^3$ | RL = -43.37 / −31. 69 dB d = 2–4.5 mm Effective bandwidth = 3.8–6.6 GHz | Electromagnetic wave absorbent | [66] |
| SiCN / N-doped CDC aerogel | Cy | Supercritical drying [$CO_2$] (5 days/ 45 °C/ 100 bar) | 450 - 1200 °C 1 h Ar | SSA = 706–1887 $m^2/g$ $V_{pore}$ = 0.21–0.97 $cm^3/g$ | $CO_2$ adsorption 3.96–4.67 mmol $g^{-1}$ @1bar, 0 °C Specific capacity ~ 140F $g^{-1}$ @10 A $g^{-1}$ for 5000 cycles | Adsorbent for $CO_2$ and EDLC | [80] |
| SiCN/Co | Cy | Freeze drying (N.A.) | 800 °C 2 h $N_2$ | Ø = 21–31 nm SSA = 54–109 $m^2/g$ $V_{pore}$ = 0.28–0.42 $cm^3/g$ | RL = -38.29/-24.31 dB d = 0.9–1.6 mm Effective bandwidth = 5.5–10.9 GHz | Microwave absorbent | [81] |
| SiCN(O) | Cy & DBE | Supercritical drying [$CO_2$] (43 °C/ 100 bar) | 1000 - 1600 °C 1 h $N_2$ | Ø = 1–48 nm SSA ~ 9–129 $m^2/g$ $V_{pore}$ = 0.04–1.05 $cm^3/g$ | N.A. | N.A. | [83] |
| SiOCN | Cy | Freeze drying (-75 °C/16 h) | 1000 °C 2 h $N_2$ | Ø = 2–100 nm SSA = 114–134 $m^2/g$ $V_{pore}$ = 0.43–0.49 $cm^3/g$ $\rho_b$ ~ 0.11–0.25 $g/cm^3$ | N.A. | Catalysis, separation, and sorption | [57] |
| SiBCN/ graphene | THF | Supercritical drying [$CO_2$] | 800 - 1200 °C 1 h $N_2$ | Ø ~ 5 nm SSA ~ 102 $m^2/g$ $V_{pore}$ = 1.43 $cm^3/g$ | $\sigma_c$ ~ 0.2 MPa | N.A. | [84] |
| SiBCN/ $ZrO_2$ | THF | Supercritical drying [$CO_2$] | 750 - 1550 °C 1 h $N_2$ | Ø = 10–70 nm SSA ~ 108–211 $m^2/g$ $V_{pore}$ = 0.49–1.57 $cm^3/g$ | N.A. | N.A. | [85] |

N.A. = Not available, Ø = pore diameter, $\phi_T$ = total porosity, SSA = specific surface area, $V_{pore}$ = Pore volume, $\rho_b$ = bulk/apparent density, RL = reflection loss, d = absorbent thickness, $\sigma_c$ = compressive strength, Cy = cyclohexane, DBE = Dibutyl ether, THF = tetrahydrofuran.

surface area reaching around 1890 $m^2/g$, was tested both for $CO_2$ adsorption (3.96–4.67 mmol.$g^{-1}$ at 1 bar, 0 °C), and electric double-layer capacitor electrode (EDLC, specific capacity of 140 F $g^{-1}$, at 10 A $g^{-1}$ for 5000 cycles) [80], see Table 2. In another study, SiCN aerogel was obtained with cobalt nanoparticles formed via reverse micro-emulsion. It was shown that the microwave absorption (MA) performance of SiCN aerogel was enhanced by the formation of cobalt in the matrix. Carbon dangling bonds and porous structure also contributed to the MA properties [81]. A peculiar study demonstrated that SiCN aerogels had unexpected out-of-furnace oxidation (due probably to the reactive silicon radicals formed at the intermediate pyrolysis temperatures) leading to an uncontrolled increase of the oxygen content of the pyrolyzed ceramics, reducing microporosity, and overall stability of the formed aerogels [65].

### 2.4. SiC-based aerogels

In the pioneering work, SiC/C aerogels were obtained by the pyrolysis of carbon-enriched (via divinylbenzene addition) polycarbosilane aerogel, see Table 3. The resultant material, suitable for surface functionalization, was anticipated to perform better for high temperature sorption and catalysis than that of the carbon aerogels in harsh environments [86]. In a recent study, a composite aerogel was produced from biphenylene-bridged polysilsesquioxane with organic intercalated (cloisite 30B) nanoclay mineral, followed by high temperature pyrolysis (1500 °C) inducing carbothermal reduction and forming SiC/C aerogels [87]. While the authors claimed after such a cumbersome process to form SiC nanowire aerogels, there was not a gel formation and therefore the formed material was a highly porous SiC monolith with 3D network of nanowires instead of an aerogel [88].

**Table 3**
Precursor type (sol-gel and commercial preceramic polymer), processing parameters, and observed properties of SiC-based aerogels.

| PDC aerogel | Processing parameters | | | Pore properties | Other properties | Possible applications | Ref. |
|---|---|---|---|---|---|---|---|
| | Solvent | Drying method | Pyrolysis | | | | |
| **Commercial preceramic polymer** | | | | | | | |
| SiC & BN | N.A. | Freeze drying (N.A.) | 1400–1500 °C<br>1–3 h<br>Ar | $\rho_b \sim 0.0001$ g/cm$^3$ | $\lambda \sim 0.002$ W m$^{-1}$ K$^{-1}$ (in vacuum @RT)<br>$\lambda \sim 0.020$ W m$^{-1}$ K$^{-1}$ (in air @RT)<br>$\alpha_l = -1.8 \times 10^{-6}$ per °C<br>$\nu = -0.25$<br>E = 25 kPa | Thermal insulation | [40] |
| SiC/C | Cy | Supercritical drying [$CO_2$] (4 days/ 50 °C/ 100 bar) | 1000–1500 °C<br>1 h<br>Ar | Ø ~ 7–500 nm<br>$\phi_T$ = 90–93%<br>SSA = 96–444 m$^2$/g<br>$V_{pore}$ = 0.31–0.79 cm$^3$/g | $\sigma_c \sim 1.6$ MPa | High temperature sorption and catalysis | [86] |
| SiC/$TiO_2$ | THF | Supercritical drying [$CO_2$] (8 h/ 45 °C/ 80 bar) | 600 - 1200 °C<br>1 h<br>$N_2$ | Ø ~ 23 nm<br>SSA = 58 m$^2$/g<br>$V_{pore}$ = 0.22 cm$^3$/g | N.A. | Catalysis, separation, and sorption | [59] |
| **Sol-gel synthesized materials** | | | | | | | |
| SiC | ACE | Supercritical drying [$CO_2$] | 700 °C<br>12 h<br>Ar | Ø ~ 9 nm<br>SSA = 232 m$^2$/g<br>$\rho_b \sim 0.157$ g/cm$^3$ | $E_g$ = 3.2 eV | Catalytic, electronic, photonic, and thermal applications | [89] |
| SiC & SiC/C | EtOH | Supercritical drying [$CO_2$] | 1500 °C<br>5 h<br>Ar | $\phi_T \sim 91$–95%<br>Ø = 1–27 nm<br>SSA = 251–892 m$^2$/g<br>$V_{pore}$ = 0.97–2.6 cm$^3$/g | N.A. | Various | [90,91] |
| SiC & SiC/C | DMF & DMA | Ambient pressure (1 day/60 °C) | 1200 - 1500 °C<br>4 h<br>Ar | $\phi_T$ = 91%<br>SSA = 796–1050 m$^2$/g<br>$V_{pore}$ = 0.64–0.80 cm$^3$/g | N.A. | Various | [92,93] |
| SiC/C | IPA | Supercritical drying [$CO_2$] | 1500 °C<br>4 h<br>Ar | $\phi_T \sim 95$–97%<br>SSA ~ 1155–2258 m$^2$/g<br>$V_{pore}$ = 3.57–6.14 cm$^3$/g | N.A. | Helium storage and catalysis | [87] |
| SiC/mullite | EtOH | Supercritical drying [$CO_2$] | 1250–1450 °C<br>5 h<br>Ar | Ø ~ 6–11 nm<br>SSA = 67–301 m$^2$/g<br>$V_{pore}$ = 0.17–0.90 cm$^3$/g | N.A. | N.A. | [94] |
| SiC/C/$SiO_2$ | EtOH | Supercritical drying [$CO_2$] | 1300–1500 °C<br>5 h<br>Ar | $\phi_T \sim 83$–89%<br>Ø ~ 5–9 nm<br>SSA = 144–746 m$^2$/g<br>$V_{pore}$ = 0.34–1.02 cm$^3$/g | $\lambda$ = 0.035–0.053 W m$^{-1}$ K$^{-1}$ @RT<br>$\sigma_c \sim 0.52$–1.86 MPa | Thermal insulation | [95] |
| SiC/C/$SiO_2$ | IPA | Ambient pressure (~3–4 days/ RT-140 °C) | 1500 °C<br>5 h<br>Ar&$N_2$ | $\phi_T \sim 86$%<br>SSA = 366–490 m$^2$/g | $\lambda \sim 0.121$ W m$^{-1}$ K$^{-1}$ @RT<br>$\sigma_c \sim 1.5$ MPa<br>E = 76 MPa | N.A. | [96,97] |
| $Si_3N_4$ | EtOH | Supercritical drying [$CO_2$] (4 h/ 50 °C/ 100 bar) | 1400–1550 °C<br>5 h<br>$N_2$ | Ø < 5 nm & >200 nm<br>SSA = 189–638 m$^2$/g<br>$V_{pore}$ = 0.84–1.74 cm$^3$/g<br>$\rho_b$ = 0.121–0.312 g/cm$^3$ | $\lambda$ = 0.045–0.061 W m$^{-1}$ K$^{-1}$ @RT | Thermal insulation | [37] |
| **Others** | | | | | | | |
| SiC nanowires (Polymer derived aerogel) | N.A. | N.A | 1300 °C<br>6 h<br>Ar | $\rho_b \sim 0.03$ g/cm$^3$<br>Nanowire diameter (D) = 80–100 nm | $\lambda$ = 0.030 W m$^{-1}$ K$^{-1}$ (in He @RT)<br>$\lambda$ = 0.230 W m$^{-1}$ K$^{-1}$ (in He @900 °C)<br>$\sigma_c$ = 0.11 MPa | Thermal insulation | [88] |
| SiC nanofiber (Polymer derived aerogel) | TBA | Freeze drying (-60 °C/48 h) | 1200–1450 °C<br>2 h<br>Ar | $\phi_T \sim 99$%<br>Nanofiber diameter (D) ~ 600 nm | $\lambda$ = 0.025–0.031 W m$^{-1}$ K$^{-1}$ @RT<br>RL = -21.41 dB @10.5 GHz<br>Effective bandwidth = 9–11.5 GHz, d = 3 mm<br>$\sigma_c \sim 0.01$–0.03 MPa<br>$\varepsilon \sim 40$% (@35 kPa) | Thermal insulation, Electromagnetic wave absorbent | [47] |

(*continued on next page*)

**Table 3** (*continued*)

| PDC aerogel | Processing parameters | | | Pore properties | Other properties | Possible applications | Ref. |
|---|---|---|---|---|---|---|---|
| | Solvent | Drying method | Pyrolysis | | | | |
| SiC nanowires (Sol-gel derived aerogel) | EtOH | Ambient pressure (5 h/100 °C) | 1550 °C<br>2 h<br>Ar | $\rho_b$ = 3–35 mg/cm$^3$<br>Nanowire diameter (D) ~ 30–280 nm | $\lambda$ ~ 0.025–0.034 W m$^{-1}$ K$^{-1}$ @RT<br>$E/E_s = 10^{-8}$-$10^{-7}$<br>Cyclic fatigue test: <20% @100 cycle | Thermal insulation | [98] |

N.A. = Not available, Ø = pore diameter, $\phi_T$ = total porosity, SSA = specific surface area, $V_{pore}$ = Pore volume, $\rho_b$ = bulk/apparent density, $\sigma_c$ = compressive strength, $\varepsilon$ = strain, $\lambda$ = thermal conductivity, $\alpha_l$ = linear thermal expansion coefficient, $\nu$ = Poisson's ratio, E = Young's modulus, $E/E_s$ = relative Young's modulus, $E_g$ = direct band gap, RL = reflection loss, d = absorbent thickness, ACE = acetone, Cy = cyclohexane, EtOH = ethanol, IPA = isopropanol, THF = tetrahydrofuran, TBA = *tert*-butanol, DMF = N,N-dimethylformamide, DMA = N,N-dimethylacetamide.

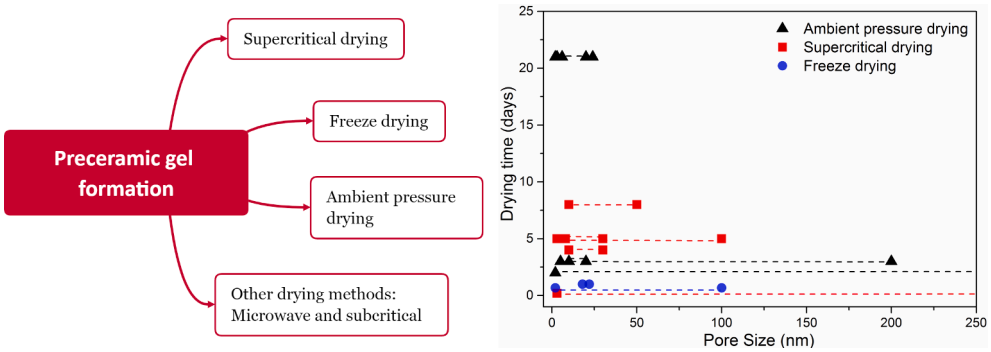


**Fig. 2.** Classification of drying methods, and the plot for drying time vs. pore size extracted from the currently available published works (note that here only the works, giving the data for both drying time and pore size which is mostly obtained from $N_2$ sorption as a distribution represented with dashed lines, are given) [37,45,57,60,63–70]. It should also be underlined that drying time is extracted as given in the works without normalization with sample dimensions.

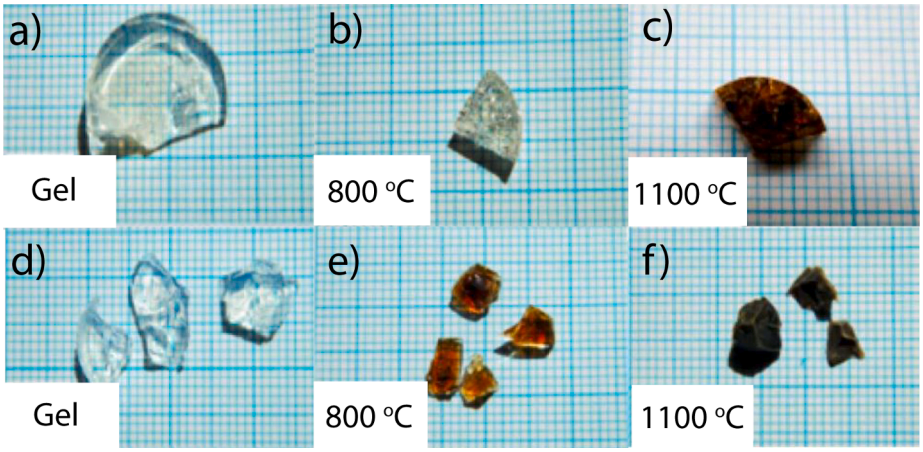


**Fig. 3.** Photographical images of the gels and aerogels pyrolyzed in hydrogen at 800–1100 °C obtained from (a–c) BTEM, and (d–f) BTEE as precursors, respectively (Reproduced from [68] with permission Royal Society of Chemistry, Copyright 2015).

In a different recent study, both SiC and BN aerogels with hyperbolic architectures were formed. These structures including nano-layered double-pane walls demonstrated to have both negative linear thermal expansion coefficient and Poisson's ratio [40]. This study, in fact, illustrated one more time how fruitful can be the PDC route to manufacture deliberately designed intricate components.

## 3. Applications of PDC aerogels

Aerogels have recently drawn considerable attention in energy storage applications, for example, carbon-based aerogels are used both as anodes and cathodes for lithium-ion [99–101], lithium-sulfur [102–104], and sodium-ion [105,106] batteries. Alternatively, they also find use in supercapacitors [107–111], an example for Mxene-rGO ($Ti_3Cr_2T_x$-reduced graphene oxide) aerogel is given in Fig. 4(a) [108]. In the same direction, sol-gel derived SiOC aerogel was tested as an anode for Li-ion batteries. The aerogel obtained by pyrolysis at 1000 °C/Ar demonstrated a reversible capacity as high as 650 mAh/g along with good cycling stability [72]. Shao et al. [112] designed a composite N-doped graphene aerogel-supported SiOC which was tested as anode for Li-ion batteries. At low charge rates, a stable reversible charge capacity of 751 mAh/g was observed, at high charge rates of 1480 mA/g, ~95% (352 mAh/g) capacity retention was achieved even after 1000 consecutive cycles. In another study [60], electrochemical properties of SiOC

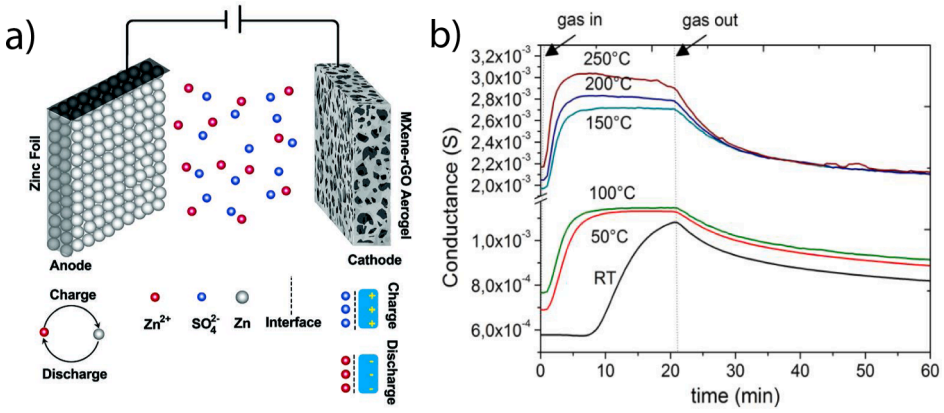


**Fig. 4.** (a) Schematic view of the energy storage system with Mxene-rGO aerogel (Reproduced from [108] with permission John Wiley and Sons, Copyright 2019), and (b) Dynamic response data of SiOC aerogel sensor to 5 ppm $NO_2$ from RT to 250 °C (Reproduced from [121] with permission Elsevier, Copyright 2014).

aerogels were examined for materials fabricated under different conditions such as solvent type (acetone or cyclohexane), pyrolysis atmosphere (Ar or Ar/$H_2$), and it was shown that the sample pyrolyzed in Ar/$H_2$ provided a high reversible capacity of 200 mAh/g at high charging/discharging rate of 20C (7200 mA/g). Zera et al. [80] produced N-doped carbide derived carbon aerogels (N-CDC) by pyrolysis of polysilazane precursor, followed by chlorine gas etching of as-formed SiCN aerogel. The N-CDC aerogel was tested as an electrode for EDLC and showed a specific capacity of 140 F $g^{-1}$, at 10 A $g^{-1}$ for 5000 cycles with no appreciable aging.

Apart from energy storage applications, due to inherent high surface area, aerogels are widely claimed to be decent purification agents (mainly adsorbent) for metal ions, oil, and other organic compounds found in the contaminated water [9,111,113–115] as well as drug delivery materials [116,117]. Bruzzoniti et al. [74] compared the adsorption behavior of PDC aerogels with foams, and demonstrated that aerogels provided higher adsorption capacity in relation to those of the foams due to higher SSA reaching 163 $m^2/g$. In another work, the metal ion adsorption efficiency of SiOC and SiCN aerogels was compared [64]. While both types of aerogels provided high adsorption capacities as 30 and 20 mg/g (after 1 h) for Cr(VI), they did not show decent sorption for Cr(III). In the same vein, the adsorption of harmful compounds in cigarette smoke was examined by using SiOCN aerogel, having a surface area of 827 $m^2/g$. The highest removal efficiency was reported to be ~76% for crotonaldehyde [79].

PDC aerogels have also been studied as biosensors [118,119], pressure [120] as well as gas (e.g. CO, $H_2$, $NO_2$, and $CO_2$) [64,67,74,79,80] sensors. The SiOC aerogel had a good response to 5 ppm $NO_2$ at 300 °C, which completely disappeared at 400 °C, and from this temperature it responded to $H_2$ [67]. Fig. 4(b) illustrates the dynamic response of SiOC aerogel sensor to 5 ppm $NO_2$ from RT to 250 °C. Dire et al. [68] suggested that transparent SiOC aerogels (SSA as 171–615 $m^2/g$) pyrolyzed under $H_2$ in between 800 and 1100 °C can be used as optical sensors for different gases.

Electromagnetic wave absorption capacity of SiCN aerogels was first analyzed by Zhao et al. [66]. Insertion of cobalt particles, the presence of carbon dangling bonds and porous structure improved the microwave absorption of Co/SiCN aerogels produced by reverse emulsion [81]. PDC aerogel made by using electrospun SiC nanofibers provided the minimum reflection loss (RL) value of −21.41 dB at 10.5 GHz [47].

Other important application fields for PDCs aerogels are inspired by the specific features of these materials which are, on one side the ultra-high temperature stability and on the other their multifunctionality. In particular, SiBCN PDCs have shown the highest thermal stability [122] as well as the highest glass transition temperature [123,124] for amorphous materials. Accordingly, thermal insulation becomes one of the most popular application areas of PDC aerogels especially at low temperatures since they provide very low thermal conductivity due to high porosity. Some materials such as silica has very low (skeleton) thermal conductivity, thus the aerogel made of it provides much lower overall thermal conductivity [125]. Such feature makes these aerogels very attractive low temperature thermal insulators to be used in refrigerator systems [126], windows [127], clothes [128]. However, while $SiO_2$ aerogels can only be used up to ca. 600 °C (above that temperature sintering causes pore collapse and densification), precursor derived SiC aerogels were shown to maintain their mesoporous structure up to 2000 °C [44].

Room temperature thermal conductivity as low as 0.027, 0.049, and 0.040 W $m^{-1}$ $K^{-1}$ were reported for sol-gel synthesized SiOC aerogel having SSA of 198 $m^2/g$ [77], sol-gel derived and supercritical dried $Si_3N_4$ aerogel [37] and sol-gel derived boron nitride/silicon oxycarbide (BN/SiOC) aerogel [70], respectively. Remarkably, even at 1300 °C the latter material demonstrates the thermal conductivity (via laser flash) as low as 0.750 W $m^{-1}$ $K^{-1}$. Likewise, Li et al. [88] showed that the thermal conductivity (measured in He) of polymer derived SiC nanowire aerogels increases from 0.030 to 0.230 W $m^{-1}$ $K^{-1}$ with increasing temperature from 25 °C to 900 °C. In another study [78], sol-gel synthesized SiBCO aerogel yielded 0.138 W $m^{-1}$ $K^{-1}$ thermal conductivity at 1500 °C (tested under vacuum). The increase in the bulk density leads to higher thermal conductivity, as recently documented for SiC nanowire aerogels in which a bulk density increase from 3 to 35 mg/$cm^3$ results in the thermal conductivity increase from 0.025 to 0.034 W $m^{-1}$ $K^{-1}$ [98].

Several potential applications of PDCs aerogels have yet not been explored. For example, PDCs possess numerous other functional properties spanning from ultra-high chemical resistance in acid and/or basic environments [129–131], high temperature piezoresistivity [132], photoluminescence [133], filtration [134], to biomedical applications [135]. Although until now there have been no reports, high temperature stable carbide- and nitride-based PDC aerogels can be used not only in those but also in several other applications, for example, as catalyst support for a highly exothermic chemical reaction such as $CO_2$ methanation, etc. [136]. While this list can be extended, we believe that the preceding examples are adequate to illustrate the wide application range. The interested reader is referred to the previous works to explore other types of aerogel utilization areas. [28,137–139].

## 4. Concluding remarks

The current status of the polymer/precursor derived ceramic (PDC) aerogels is discussed in this topical review. At present, the production techniques are not yet able to provide monolithic aerogel samples with the reasonable cost in an industrially acceptable time frame (may take several weeks to manufacture). The obtained components showed a limited range of properties, e.g., pore sizes only below 200 nm, unless

additionally treated generally few hundred $m^2/g$ specific surface area range, and poor mechanical properties, restricting the widespread use. On the other hand, various properties related to PDC aerogels, for instance, the effect of pore size or composition on the compressive strength or creep, thermal shock resistance, has not been investigated in detail yet. Ceramers -incompletely pyrolyzed preceramic polymers that combine both *cera*mic and poly*mer*ic bonds- are particular types of PDC materials with transient micro-mesoporosity formed at 600–800 °C. While some works reported the formation of such aerogels, research specifically oriented to their applications e.g., indoor air and wastewater purification is still lacking. Accordingly, systematic studies to alter the processing conditions (such as drying and pyrolysis) may affect the microstructural evolution, and therefore, mechanical, structural, and thermal properties, are needed. Beyond that certainly, new PDC aerogel compositions and systems, including composite aerogels with 1D nanostructure additions to enhance the structural integrity, should be explored. Although no study to date has specifically examined the formation of different PDC aerogel shapes (e.g. thin films, 3D printed complex parts), it is highly possible to produce aerogels in various forms by following contemporary (additive manufacturing) and traditional manufacturing processes via PDC route.

## Declaration of Competing Interest

The authors declare that they have no known competing financial interests or personal relationships that could have appeared to influence the work reported in this paper.

## Acknowledgements

Cekdar Vakif Ahmetoglu acknowledges the support of the Alexander von Humboldt (AvH) Foundation. Gian Domenico Sorarù kindly acknowledges the support from the Italian Ministry of University and Research (MIUR) within the programs PRIN2017 - 2017FCFYHK “DirectBioPower”, PRIN2017 - 2017PMR932 “Nanostructured Porous Ceramics for Environmental and Energy Applications”.

## References

[1] S.S. Kistler, Coherent expanded aerogels and jellies, Nature 127 (3211) (1931) 741, https://doi.org/10.1038/127741a0.
[2] J. Mao, J. Iocozzia, J. Huang, K. Meng, Y. Lai, Z. Lin, Graphene aerogels for efficient energy storage and conversion, Energy Environ. Sci. 11 (4) (2018) 772–799, https://doi.org/10.1039/C7EE03031B.
[3] J. Bancheri, J. Seuntjens, A. Sarfehnia, J. Renaud, Density effects of silica aerogel insulation on the performance of a graphite probe calorimeter, Med. Phys. 46 (4) (2019) 1874–1882, https://doi.org/10.1002/mp.13426.
[4] X. Hou, R. Zhang, D. Fang, Novel whisker-reinforced Al2O3–SiO2 aerogel composites with ultra-low thermal conductivity, Ceram. Int. 43 (12) (2017) 9547–9551, https://doi.org/10.1016/j.ceramint.2017.04.043.
[5] Z. Juanjuan, L. Ruiyi, L. Zaijun, L. Junkang, G. Zhiguo, W. Guangli, Synthesis of nitrogen-doped activated graphene aerogel/gold nanoparticles and its application for electrochemical detection of hydroquinone and o-dihydroxybenzene, Nanoscale 6 (10) (2014) 5458–5466, https://doi.org/10.1039/C4NR00005F.
[6] X.Y. Sun, W.B. Luo, J. Meng, X. Qing, W.Y. Fu, Y. Shuai, C.G. Wu, Monolithic pyroelectric infrared detectors using SiO2 aerogel thin films, Sens. Actuators, A Phys. 228 (2015) 69–74, https://doi.org/10.1016/j.sna.2015.03.006.
[7] H. Zhuo, Y. Hu, Z. Chen, X. Peng, L. Liu, Q. Luo, J. Yi, C. Liu, L. Zhong, A carbon aerogel with super mechanical and sensing performances for wearable piezoresistive sensors, J. Mater. Chem. A 7 (14) (2019) 8092–8100, https://doi.org/10.1039/C9TA00596J.
[8] G. Shao, O. Ovsianytskyi, M.F. Bekheet, A. Gurlo, On-chip assembly of 3D graphene-based aerogels for chemiresistive gas sensing, Chem. Commun. 56 (3) (2020) 450–453, https://doi.org/10.1039/C9CC09092D.
[9] Z. Qiu, T. Zhang, X. Yue, Y. Fang, D. Yang, F. Qiu, 3D hierarchical MnO2 aerogels with superhydrophobicity for selective oil–water separation, Appl. Organomet. Chem. 33 (9) (2019), e5073, https://doi.org/10.1002/aoc.5073.
[10] C. Jiao, T. Li, J. Wang, H. Wang, X. Zhang, X. Han, Z. Du, Y. Shang, Y. Chen, Efficient removal of dyes from aqueous solution by a porous sodium alginate/gelatin/graphene oxide triple-network composite aerogel, J. Polym. Environ. 28 (5) (2020) 1492–1502, https://doi.org/10.1007/s10924-020-01702-1.
[11] Y.X. Chen, Y. Hendrix, K. Schollbach, H.J.H. Brouwers, A silica aerogel synthesized from olivine and its application as a photocatalytic support, Constr. Build. Mater. 248 (2020), 118709, https://doi.org/10.1016/j.conbuildmat.2020.118709.
[12] M.V. Khedkar, S.B. Somvanshi, A.V. Humbe, K.M. Jadhav, Surface modified sodium silicate based superhydrophobic silica aerogels prepared via ambient pressure drying process, J. Non-Cryst. Solids 511 (2019) 140–146, https://doi.org/10.1016/j.jnoncrysol.2019.02.004.
[13] P.R. Aravind, P. Shajesh, G.D. Soraru, K.G.K. Warrier, Ambient pressure drying: a successful approach for the preparation of silica and silica based mixed oxide aerogels, J. Sol-Gel Sci. Technol. 54 (1) (2010) 105–117, https://doi.org/10.1007/s10971-010-2164-2.
[14] A.V. Rao, M.M. Kulkarni, Effect of glycerol additive on physical properties of hydrophobic silica aerogels, Mater. Chem. Phys. 77 (3) (2003) 819–825, https://doi.org/10.1016/S0254-0584(02)00207-9.
[15] D.R. Rolison, B. Dunn, Electrically conductive oxide aerogels: new materials in electrochemistry, J. Mater. Chem. 11 (4) (2001) 963–980, https://doi.org/10.1039/B007591O.
[16] E.J. Beckman, Supercritical and near-critical CO2 in green chemical synthesis and processing, J. Supercrit. Fluids 28 (2) (2004) 121–191, https://doi.org/10.1016/S0896-8446(03)00029-9.
[17] A.C. Pierre, Wet Gels and their Drying, Introduction to Sol-Gel Processing, Springer International Publishing, Cham, 2020, pp. 323–362.
[18] K. Nocentini, P. Achard, P. Biwole, M. Stipetic, Hygro-thermal properties of silica aerogel blankets dried using microwave heating for building thermal insulation, Energy Build. 158 (2018) 14–22, https://doi.org/10.1016/j.enbuild.2017.10.024.
[19] M. Sachithanadam, S.C. Joshi, Silica Aerogel Composites, Springer Singapore, 2016.
[20] Aerogels Handbook, Springer, New York, NY2011.
[21] C. Ziegler, A. Wolf, W. Liu, A.-K. Herrmann, N. Gaponik, A. Eychmüller, Modern inorganic aerogels, Angew. Chem. Int. Ed. 56 (43) (2017) 13200–13221, https://doi.org/10.1002/anie.201611552.
[22] T. Linhares, M.T. Pessoa de Amorim, L. Durães, Silica aerogel composites with embedded fibres: a review on their preparation, properties and applications, J. Mater. Chem. A 7 (40) (2019) 22768–22802, https://doi.org/10.1039/C9TA04811A.
[23] A. Du, B. Zhou, Z. Zhang, J. Shen, A special material or a new state of matter: A review and reconsideration of the aerogel, Materials 6 (3) (2013) 941–968, https://doi.org/10.3390/ma6030941.
[24] S. Karamikamkar, H.E. Naguib, C.B. Park, Advances in precursor system for silica-based aerogel production toward improved mechanical properties, customized morphology, and multifunctionality: a review, Adv. Colloid Interface Sci. 276 (2020), 102101, https://doi.org/10.1016/j.cis.2020.102101.
[25] H. Maleki, L. Durães, C.A. García-González, P. del Gaudio, A. Portugal, M. Mahmoudi, Synthesis and biomedical applications of aerogels: possibilities and challenges, Adv. Colloid Interface Sci. 236 (2016) 1–27, https://doi.org/10.1016/j.cis.2016.05.011.
[26] R. Baetens, B.P. Jelle, A. Gustavsen, Aerogel insulation for building applications: A state-of-the-art review, Energy Build. 43 (4) (2011) 761–769, https://doi.org/10.1016/j.enbuild.2010.12.012.
[27] H. Sun, Z. Xu, C. Gao, Multifunctional, ultra-flyweight, synergistically assembled carbon aerogels, Adv. Mater. 25 (18) (2013) 2554–2560, https://doi.org/10.1002/adma.201204576.
[28] A.C. Pierre, G.M. Pajonk, Chemistry of aerogels and their applications, Chem. Rev. 102 (11) (2002) 4243–4266, https://doi.org/10.1021/cr0101306.
[29] M. Li, Z. Qin, Y. Cui, C. Yang, C. Deng, Y. Wang, J.S. Kang, H. Xia, Y. Hu, Ultralight and flexible monolithic polymer aerogel with extraordinary thermal insulation by a facile ambient process, Adv. Mater. Interfaces 6 (13) (2019) 1900314, https://doi.org/10.1002/admi.201900314.
[30] X. Zhao, F. Yang, Z. Wang, P. Ma, W. Dong, H. Hou, W. Fan, T. Liu, Mechanically strong and thermally insulating polyimide aerogels by homogeneity reinforcement of electrospun nanofibers, Compos. B. Eng. 182 (2020), 107624, https://doi.org/10.1016/j.compositesb.2019.107624.
[31] S. Ghaffari Mosanenzadeh, M. Alshrah, Z. Saadatnia, C.B. Park, H.E. Naguib, Double dianhydride backbone polyimide aerogels with enhanced thermal insulation for high-temperature applications, Macromol. Mater. Eng. 305 (4) (2020) 1900777, https://doi.org/10.1002/mame.201900777.
[32] W. Fan, X. Zhang, Y. Zhang, Y. Zhang, T. Liu, Lightweight, strong, and super-thermal insulating polyimide composite aerogels under high temperature, Compos. Sci. Technol. 173 (2019) 47–52, https://doi.org/10.1016/j.compscitech.2019.01.025.
[33] J. Zhang, Y. Kong, X. Shen, Polyvinylidene fluoride aerogel with high thermal stability and low thermal conductivity, Mater. Lett. 259 (2020), 126890, https://doi.org/10.1016/j.matlet.2019.126890.
[34] K. Li, K. Wang, Y. Zhang, H. Liu, J. Wang, A polyvinylidene fluoride (PVDF)-silica aerogel (SiAG) insulating membrane for improvement of thermal efficiency during membrane distillation, J. Membr. Sci. 597 (2020), 117632, https://doi.org/10.1016/j.memsci.2019.117632.
[35] G. Luo, X. Gu, J. Zhang, R. Zhang, Q. Shen, M. Li, L. Zhang, Microstructural, mechanical, and thermal-insulation properties of poly(methyl methacrylate)/silica aerogel bimodal cellular foams, J. Appl. Polym. Sci. 134 (6) (2017) 44434, https://doi.org/10.1002/app.44434.
[36] J. Ding, X. Wu, X. Shen, S. Cui, Y. Zhong, C. An, Y. Cui, X. Chen, Synthesis and textural evolution of mesoporous Si3N4 aerogel with high specific surface area and excellent thermal insulation property via the urea assisted sol-gel technique, Chem. Eng. J. 382 (2020), 122880, https://doi.org/10.1016/j.cej.2019.122880.

[37] Y. Kong, J. Zhang, Z. Zhao, X. Jiang, X. Shen, Monolithic silicon nitride-based aerogels with large specific surface area and low thermal conductivity, Ceram. Int. 45 (13) (2019) 16331–16337, https://doi.org/10.1016/j.ceramint.2019.05.160.

[38] Z. An, R. Zhang, D. Fang, Synthesis of monolithic SiC aerogels with high mechanical strength and low thermal conductivity, Ceram. Int. 45 (9) (2019) 11368–11374, https://doi.org/10.1016/j.ceramint.2019.02.216.

[39] S. Yoon, G.D. Han, D.Y. Jang, J.W. Kim, D.H. Kim, J.H. Shim, Fabrication of yttria-stabilized zirconia aerogel for high-performance thermal barrier coating, J. Alloys Compd. 806 (2019) 1430–1434, https://doi.org/10.1016/j.jallcom.2019.07.156.

[40] X. Xu, Q. Zhang, M. Hao, Y. Hu, Z. Lin, L. Peng, T. Wang, X. Ren, C. Wang, Z. Zhao, C. Wan, H. Fei, L. Wang, J. Zhu, H. Sun, W. Chen, T. Du, B. Deng, G. J. Cheng, I. Shakir, C. Dames, T.S. Fisher, X. Zhang, H. Li, Y. Huang, X. Duan, Double-negative-index ceramic aerogels for thermal superinsulation, Science 363 (6428) (2019) 723–727, https://doi.org/10.1126/science.aav7304.

[41] B.V. Manoj Kumar, Y.-W. Kim, Processing of polysiloxane-derived porous ceramics: a review, Sci. Technol. Adv. Mater. 11 (6) (2010), 069801, https://doi.org/10.1088/1468-6996/11/6/069801.

[42] C. Vakifahmetoglu, D. Zeydanli, P. Colombo, Porous polymer derived ceramics, Mater. Sci. Eng.: R: Reports 106 (2016) 1–30, https://doi.org/10.1016/j.mser.2016.05.001.

[43] R. Riedel, G. Mera, R. Hauser, A. Klonczynski, Silicon-based polymer-derived ceramics: Synthesis properties and applications-A review, J. Ceram. Soc. JAPAN 114 (1330) (2006) 425–444, https://doi.org/10.2109/jcersj.114.425.

[44] G.D. Sorarù, E. Zera, R. Campostrini, Aerogels from preceramic polymers, in: L. Klein, M. Aparicio, A. Jitianu (Eds.), Handbook of Sol-Gel Science and Technology, Springer International Publishing, Cham, 2016, pp. 1–25.

[45] P.R. Aravind, G.D. Soraru, Porous silicon oxycarbide glasses from hybrid ambigels, Microporous Mesoporous Mater. 142 (2) (2011) 511–517, https://doi.org/10.1016/j.micromeso.2010.12.033.

[46] J.S. Downey, R.S. Frank, W.-H. Li, H.D. Stöver, Growth mechanism of poly (divinylbenzene) microspheres in precipitation polymerization, Macromolecules 32 (9) (1999) 2838–2844, https://doi.org/10.1021/ma9812027.

[47] Z. An, C. Ye, R. Zhang, P. Zhou, Flexible and recoverable SiC nanofiber aerogels for electromagnetic wave absorption, Ceram. Int. 45(17, Part B) (2019) 22793–22801. https://doi.org/10.1016/j.ceramint.2019.07.321.

[48] F.K. Chi, Carbon-containing monolithic glasses via the sol-gel process, in: W. Smothers (Ed.), Proceedings of the 7th Annual Conference on Composites and Advanced Ceramic Materials: Ceramic Engineering and Science Proceedings, 1983, pp. 704–717.

[49] A.K. Singh, C.G. Pantano, The role of Si-H functionality in oxycarbide glass synthesis, MRS Proceedings 271 (2011) 795, https://doi.org/10.1557/PROC-271-795.

[50] F. Babonneau, L. Bois, J. Livage, Silicon oxycarbides via sol-gel route: characterization of the pyrolysis process, J. Non-Cryst. Solids 147–148 (1992) 280–284, https://doi.org/10.1016/S0022-3093(05)80630-1.

[51] H. Zhang, C.G. Pantano, Synthesis and characterization of silicon oxycarbide glasses, J. Am. Ceram. Soc. 73 (4) (1990) 958–963, https://doi.org/10.1111/j.1151-2916.1990.tb05143.x.

[52] C.G. Pantano, A.K. Singh, H. Zhang, Silicon oxycarbide glasses, J. Sol-Gel Sci. Technol. 14 (1) (1999) 7–25, https://doi.org/10.1023/A:1008765829012.

[53] G.D. Sorarù, Silicon oxycarbide glasses from gels, J. Sol-Gel Sci. Technol. 2 (1) (1994) 843–848, https://doi.org/10.1007/BF00486362.

[54] A. Quaranta, A. Karakuscu, G.D. Soraru, Optical Properties, in: P. Colombo, R. Riedel, G.D. Soraru, H.-J. Kleebe (Eds.), Polymer Derived Ceramics: From Nano-Structure to Applications, DEStech Publications, INC., Lancaster, Pennsylnania, USA, 2010, pp. 253–261.

[55] C. Gervais, F. Babonneau, N. Dallabonna, G. Sorarù, Sol-gel-derived silicon-boron oxycarbide glasses containing mixed silicon oxycarbide (SiCxO4−x) and boron oxycarbide (BCyO3−y) units, J. Am. Ceram. Soc. 84 (10) (2001) 2160–2164, https://doi.org/10.1111/j.1151-2916.2001.tb00981.x.

[56] S. Dirè, R. Ceccato, S. Gialanella, F. Babonneau, Thermal evolution and crystallisation of polydimethylsiloxane-zirconia nanocomposites prepared by the sol-gel method, J. Eur. Ceram. Soc. 19 (16) (1999) 2849–2858, https://doi.org/10.1016/S0955-2219(99)00063-1.

[57] W. Zhao, G. Shao, S. Han, C. Cai, X. Liu, M. Sun, H. Wang, X. Li, R. Zhang, L. An, Facile preparation of ultralight polymer-derived SiOCN ceramic aerogels with hierarchical pore structure, J. Am. Ceram. Soc. 102 (5) (2019) 2316–2324, https://doi.org/10.1111/jace.16100.

[58] S. Aguirre-Medel, P. Jana, P. Kroll, G.D. Sorarù, Towards porous silicon oxycarbide materials: Effects of solvents on microstructural features of Poly (methylhydrosiloxane)/Divynilbenzene aerogels, Materials 11 (12) (2018) 2589, https://doi.org/10.3390/ma11122589.

[59] P. Chu, H. Liu, Y. Li, H. Zhang, J. Li, Synthesis of SiC-TiO2 hybrid aerogel via supercritical drying combined PDCs route, Ceram. Int. 42 (15) (2016) 17053–17058, https://doi.org/10.1016/j.ceramint.2016.07.213.

[60] P. Vallachira Warriam Sasikumar, E. Zera, M. Graczyk-Zajac, R. Riedel, G.D. Soraru, Structural design of polymer-derived SiOC ceramic aerogels for high-rate Li ion storage applications, J. Am. Ceram. Soc. 99(9) (2016) 2977–2983. https://doi.org/10.1111/jace.14323.

[61] M. Graczyk-Zajac, D. Vrankovic, P. Waleska, C. Hess, P.V. Sasikumar, S. Lauterbach, H.-J. Kleebe, G.D. Sorarù, The Li-storage capacity of SiOC glasses with and without mixed silicon oxycarbide bonds, J. Mater. Chem. A 6 (1) (2018) 93–103, https://doi.org/10.1039/C7TA09236A.

[62] P. Taheri, J.C. Lang, J. Kenvin, P. Kroll, Differential hysteresis scanning of non-templated monomodal amorphous aerogels, Phys. Chem. Chem. Phys. 23 (9) (2021) 5422–5430, https://doi.org/10.1039/D0CP05520D.

[63] D. Assefa, E. Zera, R. Campostrini, G.D. Soraru, C. Vakifahmetoglu, Polymer-derived SiOC aerogel with hierarchical porosity through HF etching, Ceram. Int. 42 (10) (2016) 11805–11809, https://doi.org/10.1016/j.ceramint.2016.04.101.

[64] E. Zera, E. Brancaccio, L. Tognana, L. Rivoira, M.C. Bruzzoniti, G.D. Sorarù, Reactive atmosphere synthesis of polymer-derived Si–O–C–N aerogels and their Cr adsorption from aqueous solutions, Adv. Eng. Mater. 20 (7) (2018) 1701130, https://doi.org/10.1002/adem.201701130.

[65] E. Zera, W. Nickel, S. Kaskel, G.D. Sorarù, Out-of-furnace oxidation of SiCN polymer-derived ceramic aerogel pyrolized at intermediate temperature (600–800°C), J. Eur. Ceram. Soc. 36 (3) (2016) 423–428, https://doi.org/10.1016/j.jeurceramsoc.2015.10.038.

[66] W. Zhao, G. Shao, M. Jiang, B. Zhao, H. Wang, D. Chen, H. Xu, X. Li, R. Zhang, L. An, Ultralight polymer-derived ceramic aerogels with wide bandwidth and effective electromagnetic absorption properties, J. Eur. Ceram. Soc. 37 (13) (2017) 3973–3980, https://doi.org/10.1016/j.jeurceramsoc.2017.04.068.

[67] A. Karakuscu, A. Ponzoni, P.R. Aravind, G. Sberveglieri, G.D. Soraru, Gas sensing behavior of mesoporous SiOC glasses, J. Am. Ceram. Soc. 96 (8) (2013) 2366–2369, https://doi.org/10.1111/jace.12491.

[68] S. Dirè, E. Borovin, M. Narisawa, G.D. Sorarù, Synthesis and characterization of the first transparent silicon oxycarbide aerogel obtained through H2 decarbonization, J. Mater. Chem. A 3 (48) (2015) 24405–24413, https://doi.org/10.1039/C5TA06669G.

[69] J. Ma, F. Ye, S. Lin, B. Zhang, H. Yang, J. Ding, C. Yang, Q. Liu, Large size and low density SiOC aerogel monolith prepared from triethoxyvinylsilane/tetraethoxysilane, Ceram. Int. 43 (7) (2017) 5774–5780, https://doi.org/10.1016/j.ceramint.2017.01.124.

[70] H. Yang, C. Li, X. Yue, J. Huo, F. Ye, J. Liu, F. Shi, J. Ma, New BN/SiOC aerogel composites fabricated by the sol-gel method with excellent thermal insulation performance at high temperature, Mater. Des. 185 (2020), 108217, https://doi.org/10.1016/j.matdes.2019.108217.

[71] A.H. Tavakoli, M.M. Armentrout, M. Narisawa, S. Sen, A. Navrotsky, White Si–O–C ceramic: structure and thermodynamic stability, J. Am. Ceram. Soc. 98 (1) (2015) 242–246, https://doi.org/10.1111/jace.13233.

[72] V.S. Pradeep, D.G. Ayana, M. Graczyk-Zajac, G.D. Soraru, R. Riedel, High rate capability of SiOC ceramic aerogels with tailored porosity as anode materials for Li-ion batteries, Electrochim. Acta 157 (2015) 41–45, https://doi.org/10.1016/j.electacta.2015.01.088.

[73] B. Du, C. Hong, A. Wang, S. Zhou, Q. Qu, S. Zhou, X. Zhang, Preparation and structural evolution of SiOC preceramic aerogel during high-temperature treatment, Ceram. Int. 44 (1) (2018) 563–570, https://doi.org/10.1016/j.ceramint.2017.09.212.

[74] M.C. Bruzzoniti, M. Appendini, L. Rivoira, B. Onida, M. Del Bubba, P. Jana, G. D. Sorarù, Polymer-derived ceramic aerogels as sorbent materials for the removal of organic dyes from aqueous solutions, J. Am. Ceram. Soc. 101 (2) (2018) 821–830, https://doi.org/10.1111/jace.15241.

[75] Z. Wu, X. Cheng, L. Zhang, J. Li, C. Yang, Sol-gel synthesis of preceramic polyphenylsilsesquioxane aerogels and their application toward monolithic porous SiOC ceramics, Ceram. Int. 44 (12) (2018) 14947–14951, https://doi.org/10.1016/j.ceramint.2018.05.115.

[76] M. Weinberger, S. Puchegger, T. Fröschl, F. Babonneau, H. Peterlik, N. Hüsing, Sol-gel processing of a glycolated cyclic organosilane and its pyrolysis to silicon oxycarbide monoliths with multiscale porosity and large surface areas, Chem. Mater. 22 (4) (2010) 1509–1520, https://doi.org/10.1021/cm903031d.

[77] J. Feng, Y. Xiao, Y. Jiang, J. Feng, Synthesis, structure, and properties of silicon oxycarbide aerogels derived from tetraethylortosilicate /polydimethylsiloxane, Ceram. Int. 41 (4) (2015) 5281–5286, https://doi.org/10.1016/j.ceramint.2014.11.111.

[78] X. Li, J. Feng, J. Yin, Y. Jiang, J. Feng, Preparation and properties of SiBCO aerogel and its composites, Nanomaterials 9 (1) (2019) 40, https://doi.org/10.3390/nano9010040.

[79] S. Chai, X. Dai, T. Wu, B. Liu, H. Yao, Y. Yuan, Q. Wu, Synthesis of Si/O/C/N quaternary composite aerogels with micro/mesoporous structures and their selective adsorption property for volatile carbonyl compounds in cigarette smoke, Microporous Mesoporous Mater. 301 (2020), 110164, https://doi.org/10.1016/j.micromeso.2020.110164.

[80] E. Zera, W. Nickel, G.P. Hao, L. Vanzetti, S. Kaskel, G.D. Sorarù, Nitrogen doped carbide derived carbon aerogels by chlorine etching of a SiCN aerogel, J. Mater. Chem. A 4 (12) (2016) 4525–4533, https://doi.org/10.1039/C6TA00589F.

[81] G. Shao, J. Liang, W. Zhao, B. Zhao, W. Liu, H. Wang, B. Fan, H. Xu, H. Lu, Y. Wang, R. Zhang, Co decorated polymer-derived SiCN ceramic aerogel composites with ultrabroad microwave absorption performance, J. Alloys Compd. 813 (2020), 152007, https://doi.org/10.1016/j.jallcom.2019.152007.

[82] V.L. Nguyen, E. Zera, A. Perolo, R. Campostrini, W. Li, G.D. Sorarù, Synthesis and characterization of polymer-derived SiCN aerogel, J. Eur. Ceram. Soc. 35 (12) (2015) 3295–3302, https://doi.org/10.1016/j.jeurceramsoc.2015.04.018.

[83] A. Zambotti, M. Biesuz, R. Campostrini, S.M. Carturan, G. Speranza, R. Ceccato, F. Parrino, G.D. Sorarù, Synthesis and thermal evolution of polysilazane-derived SiCN(O) aerogels with variable C content stable at 1600 °C, Ceram. Int. 47 (6) (2021) 8035–8043, https://doi.org/10.1016/j.ceramint.2020.11.157.

[84] G. An, H. Liu, H. Li, Z. Chen, J. Li, Y. Li, SiBCN ceramic aerogel/graphene composites prepared via sol-gel infiltration process and polymer-derived ceramics (PDCs) route, Ceram. Int. 46 (6) (2020) 7001–7008, https://doi.org/10.1016/j.ceramint.2019.10.267.

[85] H. Liu, G. An, H. Li, Z. Chen, J. Li, Y. Li, SiBCN-ZrO2 hybrid ceramic aerogels through the polymer-derived ceramics (PDCs) route, Ceram. Int. 44 (18) (2018) 22991–22996, https://doi.org/10.1016/j.ceramint.2018.09.098.
[86] E. Zera, R. Campostrini, P.R. Aravind, Y. Blum, G.D. Sorarù, Novel SiC/C aerogels through pyrolysis of polycarbosilane precursors, Adv. Eng. Mater. 16 (6) (2014) 814–819, https://doi.org/10.1002/adem.201400134.
[87] A. Zirakjou, M. Kokabi, SiC/C aerogels from biphenylene-bridged polysilsesquioxane/clay mineral nanocomposite aerogels, Ceram. Int. 46 (2) (2020) 2194–2205, https://doi.org/10.1016/j.ceramint.2019.09.204.
[88] B. Li, X. Yuan, Y. Gao, Y. Wang, J. Liao, Z. Rao, B. Mao, H. Huang, A novel SiC nanowire aerogel consisted of ultra long SiC nanowires, Mater. Res. Express 6 (4) (2019), 045030, https://doi.org/10.1088/2053-1591/aafaef.
[89] K. Chen, Z. Bao, A. Du, X. Zhu, G. Wu, J. Shen, B. Zhou, Synthesis of resorcinol-formaldehyde/silica composite aerogels and their low-temperature conversion to mesoporous silicon carbide, Microporous Mesoporous Mater. 149 (1) (2012) 16–24, https://doi.org/10.1016/j.micromeso.2011.09.008.
[90] Y. Kong, Y. Zhong, X. Shen, L. Gu, S. Cui, M. Yang, Synthesis of monolithic mesoporous silicon carbide from resorcinol-formaldehyde/silica composites, Mater. Lett. 99 (2013) 108–110, https://doi.org/10.1016/j.matlet.2013.02.047.
[91] Y. Kong, Y. Zhong, X. Shen, S. Cui, M. Yang, K. Teng, J. Zhang, Facile synthesis of resorcinol-formaldehyde/silica composite aerogels and their transformation to monolithic carbon/silica and carbon/silicon carbide composite aerogels, J. Non-Cryst. Solids 358 (23) (2012) 3150–3155, https://doi.org/10.1016/j.jnoncrysol.2012.08.029.
[92] G. Hasegawa, K. Kanamori, K. Nakanishi, T. Hanada, Fabrication of macroporous silicon carbide ceramics by intramolecular carbothermal reduction of phenyl-bridged polysilsesquioxane, J. Mater. Chem. 19 (41) (2009) 7716–7720, https://doi.org/10.1039/B913992C.
[93] G. Hasegawa, K. Kanamori, K. Nakanishi, T. Hanada, A New route to monolithic macroporous SiC/C composites from biphenylene-bridged polysilsesquioxane gels, Chem. Mater. 22 (8) (2010) 2541–2547, https://doi.org/10.1021/cm9034616.
[94] M. Xie, X. Wu, J. Liu, K. Zhang, In-situ synthesis and textural evolution of the novel carbonaceous SiC/mullite aerogel via polymer-derived ceramics route, Ceram. Int. 43 (13) (2017) 9896–9905, https://doi.org/10.1016/j.ceramint.2017.04.175.
[95] X. Wu, G. Shao, X. Shen, S. Cui, X. Chen, Evolution of the novel C/SiO2/SiC ternary aerogel with high specific surface area and improved oxidation resistance, Chem. Eng. J. 330 (2017) 1022–1034, https://doi.org/10.1016/j.cej.2017.08.052.
[96] M.M. Seraji, N.S. Ghafoorian, A.R. Bahramian, A. Alahbakhsh, Preparation and characterization of C/SiO2/SiC aerogels based on novolac/silica hybrid hyperporous materials, J. Non-Cryst. Solids 425 (2015) 146–152, https://doi.org/10.1016/j.jnoncrysol.2015.06.011.
[97] M.M. Seraji, N.S. Ghafoorian, A.R. Bahramian, Investigation of microstructure and mechanical properties of novolac/silica and C/SiO2/SiC aerogels using mercury porosimetry method, J. Non-Cryst. Solids 435 (2016) 1–7, https://doi.org/10.1016/j.jnoncrysol.2015.12.021.
[98] D. Lu, L. Su, H. Wang, M. Niu, L. Xu, M. Ma, H. Gao, Z. Cai, X. Fan, Scalable fabrication of resilient SiC nanowires aerogels with exceptional high-temperature stability, ACS Appl. Mater. Interfaces 11 (48) (2019) 45338–45344, https://doi.org/10.1021/acsami.9b16811.
[99] P. Angelopoulou, K. Vrettos, V. Georgakilas, G. Avgouropoulos, Graphene aerogel modified carbon paper as anode for lithium-ion batteries, ChemistrySelect 5 (9) (2020) 2719–2724, https://doi.org/10.1002/slct.201904375.
[100] R. Butt, A.H. Siddique, S.W. Bokhari, S. Jiang, D. Lei, X. Zhou, Z. Liu, Niobium carbide/reduced graphene oxide hybrid porous aerogel as high capacity and long-life anode material for Li-ion batteries, Int. J. Energy Res. 43 (9) (2019) 4995–5003, https://doi.org/10.1002/er.4598.
[101] L. Wang, G. Wei, X. Dong, Y. Zhao, Z. Xing, H. Hong, Z. Ju, Hollow α-Fe2O3 nanotubes embedded in graphene aerogel as high-performance anode material for lithium-ion batteries, ChemistrySelect 4 (38) (2019) 11370–11377, https://doi.org/10.1002/slct.201902096.
[102] X. Zhang, X. Li, W. Gao, L. Ma, H. Fang, Y. Shu, J. Ye, Y. Ding, Calixarene-functionalized porous carbon aerogels for polysulfide capture: cathodes for high performance lithium-sulfur batteries, ChemPlusChem 84 (11) (2019) 1709–1715, https://doi.org/10.1002/cplu.201900554.
[103] M. Shi, Y. Yan, Y. Wei, Y. Zou, Q. Deng, J. Wang, R. Yang, Y. Xu, T. Han, Fabrication of ultrafine Gd2O3 nanoparticles/carbon aerogel composite as immobilization host for cathode for lithium-sulfur batteries, Int. J. Energy Res. 43 (13) (2019) 7614–7626, https://doi.org/10.1002/er.4752.
[104] Y. Shu, X. Li, J. Ye, W. Gao, S. Cheng, X. Zhang, L. Ma, Y. Ding, Improved performance and immobilizing mechanism of N-doping carbon aerogel with net channel via long-chain directing for lithium–sulfur battery, Energy Technol. 8 (3) (2020) 1901057, https://doi.org/10.1002/ente.201901057.
[105] Y. Ma, Q. Wang, L. Liu, S. Yao, W. Wu, Z. Wang, P. Lv, J. Zheng, K. Yu, W. Wei, K. K. Ostrikov, Plasma-enabled ternary SnO2@Sn/Nitrogen-doped graphene aerogel anode for sodium-ion batteries, Chem. Electro. Chem. 7 (6) (2020) 1358–1364, https://doi.org/10.1002/celc.201901999.
[106] S. Hao, H. Li, Z. Zhao, X. Wang, Pseudocapacitance-enhanced anode of CoP@C particles embedded in graphene aerogel toward ultralong cycling stability sodium-ion batteries, Chem. Electro. Chem. 6 (22) (2019) 5712–5720, https://doi.org/10.1002/celc.201901549.
[107] S. Das, A.K. Nandi, Engineering of MoS2 quantum dots/PANI aerogel for high performance supercapaciator, Macromol. Symp. 386 (1) (2019) 1800242, https://doi.org/10.1002/masy.201800242.
[108] Q. Wang, S. Wang, X. Guo, L. Ruan, N. Wei, Y. Ma, J. Li, M. Wang, W. Li, W. Zeng, MXene-reduced graphene oxide aerogel for aqueous zinc-ion hybrid supercapacitor with ultralong cycle life, Adv. Electron. Mater. 5 (12) (2019) 1900537, https://doi.org/10.1002/aelm.201900537.
[109] Z. Zhai, B. Ren, Y. Zheng, Y. Xu, S. Wang, L. Zhang, Z. Liu, Nitrogen-containing carbon aerogels with high specific surface area for supercapacitors, Chem. Electro. Chem. 6 (24) (2019) 5993–6001, https://doi.org/10.1002/celc.201901951.
[110] H. Li, J. Li, A. Thomas, Y. Liao, Ultra-high surface area Nitrogen-doped carbon aerogels derived from a schiff-base porous organic polymer aerogel for CO2 storage and supercapacitors, Adv. Funct. Mater. 29 (40) (2019) 1904785, https://doi.org/10.1002/adfm.201904785.
[111] Z. Xie, J. Zhu, Y. Bi, H. Ren, X. Chen, H. Yu, Nitrogen-doped porous graphene-based aerogels toward efficient heavy metal ion adsorption and supercapacitor applications, Phys. Status Solidi RRL 14 (1) (2020) 1900534, https://doi.org/10.1002/pssr.201900534.
[112] G. Shao, D.A.H. Hanaor, J. Wang, D. Kober, S. Li, X. Wang, X. Shen, M.F. Bekheet, A. Gurlo, Polymer-derived SiOC integrated with a graphene aerogel as a highly stable Li-ion battery anode, ACS Appl. Mater. Interfaces 12 (41) (2020) 46045–46056, https://doi.org/10.1021/acsami.0c12376.
[113] Z. Shariatinia, A. Esmaeilzadeh, Hybrid silica aerogel nanocomposite adsorbents designed for Cd(II) removal from aqueous solution, Water Environ. Res. 91 (12) (2019) 1624–1637, https://doi.org/10.1002/wer.1162.
[114] M. Peydayesh, M.K. Suter, S. Bolisetty, S. Boulos, S. Handschin, L. Nyström, R. Mezzenga, Amyloid fibrils aerogel for sustainable removal of organic contaminants from water, Adv. Mater. 32 (12) (2020) 1907932, https://doi.org/10.1002/adma.201907932.
[115] J. Liu, H. Yang, K. Liu, R. Miao, Y. Fang, Gel-emulsion-templated polymeric aerogels for water treatment by organic liquid removal and solar vapor generation, ChemSusChem 13 (4) (2020) 749–755, https://doi.org/10.1002/cssc.201902970.
[116] S. Wei, Y.C. Ching, C.H. Chuah, Synthesis of chitosan aerogels as promising carriers for drug delivery: A review, Carbohydr. Polym. 231 (2020), 115744, https://doi.org/10.1016/j.carbpol.2019.115744.
[117] Z. Ulker, C. Erkey, An emerging platform for drug delivery: Aerogel based systems, J. Control. Release 177 (2014) 51–63, https://doi.org/10.1016/j.jconrel.2013.12.033.
[118] Z. Ma, P. Song, Z. Yang, Q. Wang, Trimethylamine detection of 3D rGO/mesoporous In2O3 nanocomposites at room temperature, Appl. Surf. Sci. 465 (2019) 625–634, https://doi.org/10.1016/j.apsusc.2018.09.233.
[119] C. Rajkumar, P. Veerakumar, S.M. Chen, B. Thirumalraj, S.B. Liu, Facile and novel synthesis of palladium nanoparticles supported on a carbon aerogel for ultrasensitive electrochemical sensing of biomolecules, Nanoscale 9 (19) (2017) 6486–6496, https://doi.org/10.1039/c7nr00967d.
[120] X. Chen, H. Liu, Y. Zheng, Y. Zhai, X. Liu, C. Liu, L. Mi, Z. Guo, C. Shen, Highly compressible and robust polyimide/carbon nanotube composite aerogel for high-performance wearable pressure sensor, ACS Appl. Mater. Interfaces 11 (45) (2019) 42594–42606, https://doi.org/10.1021/acsami.9b14688.
[121] A. Karakuscu, A. Ponzoni, D. Ayana, G.D. Soraru, G. Sberveglieri, High carbon-high porous SiOC glasses for room temperature NO2 sensing, Procedia Eng. 87 (2014) 160–163, https://doi.org/10.1016/j.proeng.2014.11.608.
[122] R. Riedel, A. Kienzle, W. Dressler, L. Ruwisch, J. Bill, F. Aldinger, A silicoboron carbonitride ceramic stable to 2,000°C, Nature 382 (6594) (1996) 796–798, https://doi.org/10.1038/382796a0.
[123] T. Rouxel, G. Massouras, G.-D. Sorarù, High temperature behavior of a gel-derived SiOC glass: Elasticity and viscosity, J. Sol-Gel Sci. Technol. 14 (1) (1999) 87–94, https://doi.org/10.1023/A:1008779915809.
[124] R. Riedel, L.M. Ruswisch, L. An, R. Raj, Amorphous silicoboron carbonitride ceramic with very high viscosity at temperatures above 1500 C, J. Am. Ceram. Soc. 81 (12) (1998) 3341–3344, https://doi.org/10.1111/j.1151-2916.1998.tb02780.x.
[125] C. Bi, G.H. Tang, Effective thermal conductivity of the solid backbone of aerogel, Int. J. Heat Mass Transf. 64 (2013) 452–456, https://doi.org/10.1016/j.ijheatmasstransfer.2013.04.053.
[126] G.G. Iliş, Experimental insulation performance evaluation of aerogel for household refrigerators, in: I. Dincer, A. Midilli, H. Kucuk (Eds.), Progress in Exergy, Energy, and the Environment, Springer International Publishing, Cham, 2014, pp. 495–506.
[127] D. Li, C. Zhang, Q. Li, C. Liu, M. Arıcı, Y. Wu, Thermal performance evaluation of glass window combining silica aerogels and phase change materials for cold climate of China, Appl. Therm. Eng. 165 (2020), 114547, https://doi.org/10.1016/j.applthermaleng.2019.114547.
[128] M. Ibrahim, K. Nocentini, M. Stipetic, S. Dantz, F.G. Caiazzo, H. Sayegh, L. Bianco, Multi-field and multi-scale characterization of novel super insulating panels/systems based on silica aerogels: thermal, hydric, mechanical, acoustic, and fire performance, Build Environ. 151 (2019) 30–42, https://doi.org/10.1016/j.buildenv.2019.01.019.
[129] G.D. Sorarù, S. Modena, E. Guadagnino, P. Colombo, J. Egan, C. Pantano, Chemical durability of silicon oxycarbide glasses, J. Am. Ceram. Soc. 85 (6) (2002) 1529–1536, https://doi.org/10.1111/j.1151-2916.2002.tb00308.x.
[130] T. Semerci, M.D. de Mello Innocentini, G.A. Marsola, P.R.O. Lasso, G.D. Soraru, C. Vakifahmetoglu, Hot air permeable preceramic polymer derived reticulated ceramic foams, ACS Appl. Polym. Mater. 2 (9) (2020) 4118–4126, https://doi.org/10.1021/acsapm.0c00734.

[131] C. Vakifahmetoglu, T. Semerci, G.D. Soraru, Closed porosity ceramics and glasses, J. Am. Ceram. Soc. 103 (5) (2020) 2941–2969, https://doi.org/10.1111/jace.16934.
[132] K. Terauds, P.E. Sanchez-Jimenez, R. Raj, C. Vakifahmetoglu, P. Colombo, Giant piezoresistivity of polymer-derived ceramics at high temperatures, J. Eur. Ceram. Soc. 30 (11) (2010) 2203–2207, https://doi.org/10.1016/j.jeurceramsoc.2010.02.024.
[133] A. Karakuscu, R. Guider, L. Pavesi, G.D. Sorarù, White luminescence from sol-gel-derived SiOC thin films, J. Am. Ceram. Soc. 92 (12) (2009) 2969–2974, https://doi.org/10.1111/j.1551-2916.2009.03343.x.
[134] D. Zeydanli, S. Akman, C. Vakifahmetoglu, Polymer-derived ceramic adsorbent for pollutant removal from water, J. Am. Ceram. Soc. 101 (6) (2018) 2258–2265, https://doi.org/10.1111/jace.15423.
[135] M. Arango-Ospina, F. Xie, I. Gonzalo-Juan, R. Riedel, E. Ionescu, A.R. Boccaccini, Review: Silicon oxycarbide based materials for biomedical applications, Appl. Mater. Today 18 (2020), 100482, https://doi.org/10.1016/j.apmt.2019.100482.
[136] J. Wang, A. Gili, M. Grünbacher, S. Praetz, J.D. Epping, O. Görke, G. Schuck, S. Penner, C. Schlesiger, R. Schomäcker, A. Gurlo, M.F. Bekheet, Silicon oxycarbonitride ceramic containing nickel nanoparticles: from design to catalytic application, Mater. Adv. 2 (5) (2021) 1715–1730, https://doi.org/10.1039/D0MA00917B.
[137] D. Karami, A review of aerogel applications in adsorption and catalysis, J. Pet. Sci. Technol. 8 (4) (2018) 3–15, https://doi.org/10.22078/jpst.2018.3348.1535.
[138] J. Stergar, U. Maver, Review of aerogel-based materials in biomedical applications, J. Sol-Gel Sci. Technol. 77 (3) (2016) 738–752, https://doi.org/10.1007/s10971-016-3968-5.
[139] J.-H. Lee, S.-J. Park, Recent advances in preparations and applications of carbon aerogels: A review, Carbon 163 (2020) 1–18, https://doi.org/10.1016/j.carbon.2020.02.073.